Study on Seepage for Random Packed Porous Media Using the Lattice Boltzmann Method

Jinfeng Zhang[1,2], Zhongyue Li[1], Guangwei Liu[1*], and Qinghe Zhang[1]

[1]State Key Laboratory of Hydraulic Engineering Simulation and Safety, Tianjin University, Tianjin, 300072, China

[2]Key Laboratory of Earthquake Engineering Simulation and Seismic Resilience of China Earthquake Administration, Tianjin University, Tianjin, 300350, China

Corresponding author: Guangwei Liu (guangweiliu@tju.edu.cn)

Key Points:

- DNS to study the permeability coefficient for the laminar and turbulent seepage flow.
- The porosity, particle size, particle size distribution and Reynold number can affect the permeability coefficient.
- A modified formulation for the permeability coefficient is significant for porous medium seepage.

Abstract

The permeability coefficient of seepage is an important factor that is widely used in various engineering fields. There are numerous issues that influence the permeability coefficient, among which the porosity, particle size, particle size distribution and Reynolds number are of great importance. In this paper, a C++ code based on the three-dimensional lattice Boltzmann method (LBM) was developed and used to investigate the effects of the abovementioned factors on the permeability coefficient. A multiple relaxation time (MRT) collision scheme of the LB equations was used in the simulation. Porous media were prepared using the random packing method. Laminar flow and turbulent flow were simulated separately for particle Reynolds numbers in a range from 0.001 to 3,000. It was proven that in addition to the influence of porosity and particle size distribution on the permeability, the influence of the Reynolds number was obvious and could not be ignored. As the Reynolds number increased, the permeability of porous media decreased gradually. Based on the numerical simulation results, a modified formula for the permeability coefficient is proposed.

1. Introduction

Seepage phenomena play important roles in permeable seabeds and breakwaters. The seepage of water through a sandy seabed beneath a breakwater is an important consideration for its design and stability. However, the permeability of seepage is difficult to predict because of the complexity of pore geometric characteristics and

pore connectivity.

Many scholars have conducted research on permeability through analytical studies, experiments, field observations and numerical simulations. For example, an experiment can be a simple way to calculate permeability by measuring the pressure gradient and the flow rate (Despois and Mortensen, 2005; Rodríguez et al., 2004). For saturated flow at a low Reynolds number, the mean flow rate of a viscous fluid through a porous medium is inversely proportional to the viscosity and proportional to the applied pressure difference. Darcy's law can be written as

$$-\frac{dP}{dx} = \frac{1}{K} \cdot (\mu \cdot V) \tag{1}$$

where $\frac{dP}{dx}$ is the pressure gradient, K is the permeability coefficient, μ is the dynamic viscosity coefficient of the fluid, and V is the overall mean value of the velocity in the x direction. The dimension of relative permeability K is length squared.

However, as velocities quicken, discrepancies between experimental data and results obtained from Darcy's law appear. A term representing kinetic energy is suggested to be added to Eq. 1:

$$-\frac{dP}{dx} = \frac{1}{K} \cdot (\mu \cdot V) + \beta \cdot (\rho \cdot V^2) \tag{2}$$

where β is the Forchheimer coefficient (also known as the non-Darcy coefficient) and ρ is the density of the fluid.

The determination of parameters is very important. The available literature provides many general formulas to calculate permeability and Forchheimer coefficients based on porous media parameters such as porosity or tortuosity, but the formulas are usually empirical and not universal (Sobieski and Trykozko, 2014).

Different formulas computed with a fixed set of parameters can lead to totally different β coefficient values, ranging over several orders of magnitude.

Based on experimental data and theoretical analysis, the classic Kozeny–Carman (KC) equation (Carman, 1997, 1939) that relates the permeability K to porosity ε has been proposed:

$$K = \frac{\varepsilon^3}{C_{KC} \Gamma^2 S^2} \tag{3}$$

where C_{KC} is the Kozeny coefficient, Γ is the hydraulic tortuosity, which can be defined as the ratio of the average length of the fluid paths to the geometric length of the porous media (Matyka et al., 2008), and S is the specific surface area.

To predict the permeability properly, many different forms of modified KC equations have been developed. Koponen (Koponen et al., 1996) proposed the concept of effective porosity, which is defined as the ratio of the volume of the conducting pores to the total pore volume, to replace the original porosity in Eq. 1. He considered that some pores were interconnected and contributed very little or nothing to the global flow. Later, Koponen (Koponen et al., 1997) used the lattice-gas cellular automaton method to simulate an uncompressible flow in a 2D porous medium and gave the relationship between effective porosity and original porosity. However, compared to a 2D porous medium, the structure of a 3D porous medium is more complicated. 2D simulations cannot consider the real pore connectivity. The empirical formula of the 2D model is not practical. Sheikh (Sheikh and Pak, 2015) gave a new empirical formula of the effective porosity for 3D conditions using the lattice

Boltzmann method. However, some parameters for his empirical formula are not easily obtained.

The geometric characteristic is also a key factor that influences the permeability of the pore medium. Some researchers have used regularly arranged spheres or cylinders (Li et al., 2005; Okabe and Blunt, 2004), whereas others have used random packed methods (Lee and Yang, 1997; Maier et al., 1998) to build porous media with simple geometric features to study permeability. Their results have shown that different arrangements of particles can cause different permeabilities. Some studies of the influence of particle shape on the permeability of a porous medium through numerical simulations have been carried out in the past (Dorai et al., 2015; Osiptsov, 2017; Saomoto and Katagiri, 2015; Scholes et al., 2007; Stewart et al., 2006). These studies used regularly shaped particles such as cubes or ellipsoids. Chukwudozie (Chukwudozie and Tyagi, 2013) simulated the effect of the surface geometric characteristics of particles on permeability. In their study, the surface geometric characteristics of particles were controlled by the several bulges above the sphere, and the particle arrangement in the porous medium was cubic and centred as a regular body, which is very different from the real arrangement condition. Natural soil particles can be regarded as a set of spheres with a random size distribution that reflect realistic conditions. Liu (Liu and Jeng, 2019) used two parameters (Wadell sphericity and Cox roundness) to express the roughness of spherical particles. Their simulation results showed that the sensitivity of sphericity and roundness is less than that of particle size distribution and porosity.

In previous studies, simulations have mainly focused on uniform particle size. However, soil is composed of various particle sizes. Smaller particles may have more influence on permeability due to their greater specific surface area (Ghassemi and Pak, 2011), so the size distribution of particles must be considered (Wilson et al., 2008). In summary, although there are many formulas for predicting permeability using geometric parameters, only a few can be used in engineering practice. The empirical formulas proposed in the existing studies are diverse, lack a general format, and can be applied only to special soils.

Previous studies have mainly focused on investigating the permeability of laminar flow through porous media while neglecting the characteristics of turbulent flow. This is mainly because of the complexities of the flow field in porous media and the significant computational resources required for simulating turbulence. However, understanding the behaviour of turbulent flow is crucial. Fattahi (Fattahi et al., 2016) employed a lattice Boltzmann method to investigate high Reynolds number flow through an unstructured packing of spherical particles, but a comprehensive analysis of the permeability regularities was not conducted. In this study, we present a three-dimensional numerical simulation using a multiple relaxation time lattice Boltzmann method to examine the flow through a soil medium composed of rigid spherical particles with a certain size distribution. Through numerical simulations, we establish correlations between parameters such as porosity, particle size distribution, Reynolds number, and permeability.

Many researchers have used numerical simulation methods to study porous

media (Bogdanov et al., 2003; Hasanov et al., 2020). Traditional numerical simulation methods cannot manage the complex boundary conditions of porous media. The lattice Boltzmann method (LBM) proposed by McNamara and Zanetti (McNamara and Zanetti, 1988) is a mesoscopic simulation method that combines macroscopic continuous simulation and microscopic molecular dynamics simulation. It is a conventional approach used to simulate the seepage of porous media. In addition to the lattice Boltzmann method, some researchers have used the finite volume method (FVM) to study permeability at the pore scale (Garcia et al., 2009; Stefansson and Keilegavlen, 2023; Torskaya et al., 2014). The disadvantage of the finite volume method is that the general simulation conditions are relatively sparse because of the complexity of FVM modelling. Furthermore, owing to the high computational resource cost of solving the Navier–Stokes (N–S) equations, most of these studies have employed calculations based on the Laplace equation instead of the N–S equations.

The following work is structured as follows: Section 2 presents the numerical model, which is divided into two parts: the lattice Boltzmann method (Section 2.1) and the construction of porous media (Section 2.2). The validation of the presented numerical model is discussed in Section 2.3. Section 3 provides a comparison of the numerical results. Finally, Section 4 presents the conclusions of this study.

2. Numerical Model and Validation

2.1 Lattice Boltzmann method for fluid flows

The LBM is a conventional computational fluid method based on the lattice gas automaton method and the Boltzmann equation. This method is a mesoscopic simulation method and has a clear physical background based on molecular dynamics theory. The advantage of the LBM in seepage problems lies with its strong capability to simulate complex pore structures (Chen and Doolen, 1998).

The Bhatnagar–Gross–Krook (BGK) model is the most popular LB method with a standard bounce-back scheme for fluid–solid boundary conditions (Guo et al., 2000). In the BGK model, the collision operator is approximated by a single relaxation time (SRT) approximation. However, the SRT approximation has some disadvantages, such as numerical instability and viscosity dependence at boundary locations. The dependence on viscosity causes some problems in seepage simulations. The permeability becomes viscosity dependent, even though it should be a physical property of the porous medium alone. By using a multiple relaxation time (MRT) approach, which separates the relaxation times for different kinetic nodes, the disadvantage of the BGK model can be significantly overcome to improve numerical stability (Du et al., 2006; Pape et al., 2000). The general form of the governing equation with the D3Qq velocity set in the MRT model is as follows:

$$f_\alpha\left(\mathbf{x}+\mathbf{e}_a\Delta t, t+\Delta t\right)-f_\alpha\left(\mathbf{x},t\right)=-\mathbf{M}^{-1}\left[\mathbf{S}\left(\mathbf{m}-\mathbf{m}^{eq}\right)\right] \tag{4}$$

where $f_\alpha\left(\mathbf{x},t\right)$ denotes the density distribution function at lattice position x and time t; $\mathbf{e}_a$ is the discrete velocity in the α direction, and α ranges from 1 to q-1 in three dimensions. The particle speed is c=$\Delta x/\Delta t$, Δx is the lattice constant, and Δt is the time step. **M** is the transformation matrix. **S** is the diagonal collision matrix in moment

space. **m** is the vector of moments. $\mathbf{m}^{eq}$ is the vector of equilibrium moments.

The equilibrium distribution function of the D3Q27 model is

$$f_\alpha^{eq} = \omega_\alpha \rho + \omega_\alpha \rho_0 \left[\frac{\mathbf{e}_\alpha \cdot \mathbf{u}}{c_s^2} + \frac{(\mathbf{e}_\alpha \cdot \mathbf{u})^2}{2c_s^4} - \frac{|\mathbf{u}|^2}{2c_s^2} \right] \tag{5}$$

where c_s is the lattice sound speed ($c_s^2 = c^2/3$), ρ_0 is the reference density of the fluid and ω_α is the weight coefficient, which has the following value:

$$\omega_0 = \frac{8}{27},\ \omega_{1-6} = \frac{2}{27},\ \omega_{7-18} = \frac{1}{54},\ \omega_{19-26} = \frac{1}{216} \tag{6}$$

The macro density and velocity can be obtained through the distribution function:

$$\rho = \sum_\alpha f_\alpha \tag{7}$$

$$\rho_0 \mathbf{u} = \sum_\alpha f_\alpha \mathbf{e}_\alpha \tag{8}$$

where ρ is the fluid density and **u** is the vector of fluid velocity.

Eq. (2) can be restored to the Navier–Stokes equation based on the Chapman–Enskog expansion (Liu et al., 2021).

The Smagorinsky eddy viscosity model (Krafczyk and Olke, 2003) is used to simulate turbulent flows, and then the LBE large eddy simulation (LES) model is established. The eddy viscosity υ_t is calculated by the mean strain rate $\bar{\mathbf{S}}$,

$$\upsilon_t = (C_s \Delta)^2 \left\| \bar{\mathbf{S}} \right\| \tag{9}$$

where C_s = 0.15 is the Smagorinsky constant, $\Delta = \delta_x$ is the filter length, and $\left\| \bar{\mathbf{S}} \right\| = \sqrt{2\bar{S}_{ij}\bar{S}_{ij}}$.

In the LBE, the mean strain rate $\bar{\mathbf{S}}$ is calculated by the nonequilibrium part of the mean second-order moment $\bar{\mathbf{\Pi}}$:

$$\bar{S}_{ij} = \frac{3\bar{\Pi}_{ij}}{-2\tau_{total}\rho_0 c^2 \delta_t} \tag{10}$$

where $\bar{\Pi}_{ij} = \sum_{\alpha=0}^{q-1} \mathbf{e}_{\alpha i}\mathbf{e}_{\alpha j} f_\alpha - \rho_0 u_i u_j - p\delta_{ij}$.

In our simulations, the pressure gradient boundary condition is applied to the inlet and outlet boundary. On the solid–fluid surface, the central linear interpolation (CLI) scheme of boundary conditions is applied. The CLI scheme was proposed by Ginzburg (d'Humières et al., 2002; Ginzburg et al., 2008; Ginzburg and d'Humières, 2003) based on two relaxation times (TRT), which can be seen as the minimal configuration that provides just enough free relaxation parameters to avoid nonlinear dependencies of the truncation errors on the viscosity in the context of porous media simulations.

Let $\mathbf{x}_{f_i}$ denote a lattice node located at a distance of at most $i > 0$ cells from the boundary, and let $q = \left|\mathbf{x}_{f_1} - \mathbf{x}_w\right| / \left|\mathbf{x}_{f_1} - \mathbf{x}_b\right|$ define a normalized wall distance (Fig. 1). The CLI scheme requires three values at two fluid nodes. The CLI scheme can be expressed as

$$f_\beta(\mathbf{x}_{f1}, t) = \frac{1-2q}{1+2q} f_\alpha(\mathbf{x}_{f1}, t) - \frac{1-2q}{1+2q} f_\beta(\mathbf{x}_{f1} - \mathbf{e}_\alpha \delta_t, t) + f_\alpha(\mathbf{x}_{f1} + \mathbf{e}_\alpha \delta_t, t) \tag{11}$$

where β is the diametrically opposite direction to α.

To verify the developed MRT–LBM model and the given boundary conditions, the Poiseuille flow between two parallel plates is simulated. Between the two parallel plates, the velocities at the plates are zero, and the velocity reaches its maximum in the middle. The velocity profile between two plates of width $2a$ is a parabolic curve given by

$$u(y) = \frac{\Delta p}{2\nu\rho L}\left(a^2 - y^2\right) \tag{12}$$

where L is the length along the low direction, v is the fluid dynamic viscosity, Δp is the pressure difference, and y is the distance of any point from the middle of the domain.

The maximum velocity along the centreline is given by

$$u_0 = \frac{\Delta p a^2}{2\nu\rho L} \tag{13}$$

The lattice sizes of the calculation domain are set to 100×100×200, and the Reynolds number is 0.1, which indicates that the flow is laminar. The velocity contour and the comparison between the numerical results and analytical solutions of the velocity in the x direction are shown in Fig. 2.

2.2 Simulation of porous medium

Simulation methods for forming granular packings of hard particles usually involve one of two methods. One is the concurrent algorithm, which involves the densification of a fixed number of particles. The other is the sequential algorithm, which involves progressively adding more particles to a fixed volume.

The sphere packing code utilizes the concurrent algorithm used by Williams and Philipse to generate packings of spherocylinders (Williams and Philipse, 2003). The algorithm has been modified to support the generation of packings for systems of spheres with lognormally distributed radii and to provide control over the final porosity of the packing. The major steps can be seen in Fig. 3.

To improve convergence, the spheres are divided into a collection of cells consisting of equally sized subdomains, which is a common optimization for N-particle methods. To consider potential overlaps only from neighbouring cells for a given sphere, the code is significantly accelerated by increasing the number of cells, thereby reducing the length of the search path needed when computing overlaps. However, this optimization can lead to oversights in overlap computation if the maximum radius exceeds half of the cell width. Errors may occur if too many cells are requested for a given system, causing the maximum radius to exceed half of the cell width. Nonetheless, the generated porous medium is consistent with the actual on-site conditions. Fig. 4 illustrates the typical porous media constructed in the study.

2.3 Simulation of seepage in the porous medium

The boundary conditions in the simulation domain are set as follows: the pressure boundary condition is used for the inlet boundary and the outlet boundary. The CLI scheme boundary condition (Ginzburg et al., 2008; Ginzburg and d'Humières, 2003) is used for the other four boundaries and the boundaries of the solid particles. The simulation domain is set to 200×200×200, and the porosity ε is 0.5.

The relative permeability can be calculated by Eq. 1. The dimensionless permeability k is defined as

$$k = \frac{K}{d_p^{\,2}} \tag{14}$$

where d_p is the characteristic length of the spherical particles. For the seepage of

porous media, the medium particle size d_{50} is generally used to denote the characteristic length.

For the Poiseuille flow between two parallel plates filled with a porous medium of porosity ε, the Navier–Stokes equation can be simplified as

$$\frac{\nu}{\varepsilon}\frac{\partial^2 \mathrm{u}}{\partial \mathrm{y}^2}+\frac{\mathbf{F}}{\varepsilon}=0 \tag{15}$$

where **F** denotes the total body force due to the porous media and other external force fields and is given by

$$\mathbf{F}=-\frac{\varepsilon\nu}{K}\mathbf{u}-\frac{\varepsilon F_{\varepsilon}}{\sqrt{K}}|\mathbf{u}|\mathbf{u}+\varepsilon\mathbf{G} \tag{16}$$

where **G** is the body force induced by the external force. F_ε is the geometric function and is related to the porosity ε. On the right side of Eq. 16, the first term is the linear (Darcy) and the second term is the nonlinear (Forchheimer) drag due to the porous medium.

The velocity of the solid–fluid boundary is zero, and the lateral velocity component v is zero everywhere. The quadratic nature of the nonlinear drag makes it negligible for low-velocity flows. For the cases in which the Reynolds number is small, the nonlinear drag can be neglected. Without the nonlinear term, the analytical solution of Eq. 15 can be written as

$$u=\frac{GK}{\nu}\left(1-\frac{\cosh[r(y-H/2)]}{\cosh(rH/2)}\right) \tag{17}$$

where u_0 is the peak velocity of the flow along the centreline given by

$$u_0=\frac{GK}{\nu}\left[1-\cosh^{-1}\left(\frac{rH}{2}\right)\right] \tag{18}$$

where $r = \sqrt{\nu / K}$.

Due to the presence of solid particles, the velocity distribution of a single line may deviate from the analytical solution. Therefore, to more accurately compare with the analytical solution, the mean velocity of the cross section at height *y* is calculated as a replacement for the local velocity at that particular location. The comparison between the numerical results and analytical solutions of the velocity in the *y* direction is shown in Fig. 5(a). The analytical solutions are calculated by Eq. 18, and the simulation results are the mean velocity of the cross section in the height *y*. Because of the randomness of the sphere pack structure, the mean velocity distribution of the porous seepage may not fit the analytical solutions accurately. The maximum error of the velocity is 10.6%.

Fig. 5(b) shows the streamlines of the simulated porous medium. In pore spaces, streamlines often undergo changes, particularly in the regions between large and small particles. Between large particles, streamlines tend to become more tortuous and complex, as the large particles impede fluid flow and cause streamlines to bend and branch. Between small particles, streamlines tend to become smoother and more linear, as the gaps between small particles are smaller and fluid can more easily pass through these gaps and flow along relatively straight paths.

Sobieski (Sobieski and Trykozko, 2014) calculated the permeability and Forchheimer coefficient based on experimentally measured flow rates and pressure drops. Fig. 6 illustrates the comparison of the velocity–pressure relationship between the experimental data and simulation data. The simulation data are in good agreement

300 with the experimental data. The simulation parameters are based on Sobieski's
301 experiment and are summarized in Table 1. The maximum error between the
302 simulation results and experimental results is 6%. The main reason for the error is
303 attributed to the unclear characteristics of certain porous media, such as the
304 nonuniform coefficient.
305
306 **2.4 Mesh sensitivity analysis**
307 The minimum resolution of each spherical particle required for simulation
308 accuracy needs to be determined. Under the situation of porosity ε = 0.5, the
309 permeability of spherical particles with different resolutions (d_p/dx) is shown in Fig. 7.
310 Fig. 7 illustrates that when the diameters of medium spherical particles reach ten
311 lattices, the dimensionless permeability will remain stable. Twenty lattices are
312 sufficient to describe the structure of spherical particles.
313
314 **3. Results and Discussion**
315 **3.1 Effect of porosity on permeability**
316 To study the effect of porosity on permeability, it is necessary to ensure that other
317 parameters remain unchanged. The porosity is adjusted by controlling the number of
318 particles, and the floc size distribution remains unchanged. The medium floc diameter
319 was fixed at 20 lattice units, and the particle numbers were set to 1000. Considering
320 the porosity of natural soil, the upper limit of porosity was set to 0.55. Nine porous
321 media with different porosities varying from 0.35 to 0.55 were constructed. Their

322 permeabilities were simulated and calculated.

323 The widely used form of the KC equation is obtained as (Chen and Doolen,

324 1998)

325 $$K = \frac{\varepsilon^3}{(1-\varepsilon)^2}\frac{{d_p}^2}{180} \quad (19)$$

326 Sheikh (Sheikh and Pak, 2015) summarized another equation, which after some

327 substitutions becomes

328 $$K = \frac{1-1.209(1-\varepsilon)^{2/3}}{60\varepsilon}\frac{\varepsilon^3}{(1-\varepsilon)^2}{d_p}^2 \quad (20)$$

329 Recently, Ahmadi (Ahmadi et al., 2011) provided the following relationship by

330 analytical derivation:

331 $$K = \frac{1-1.209(1-\varepsilon)^{2/3}}{30[1-1.209(1-\varepsilon)^{2/3}+2\varepsilon](1-\varepsilon)^2}\frac{\varepsilon^3}{(1-\varepsilon)^2}{d_p}^2 \quad (21)$$

332 Jeong's equation (Jeong, 2010) is as follows:

333 $$K = e^{(0.709\ln(\varepsilon^{11/3}/(1-\varepsilon)^2)-5.09)}{d_p}^2 \quad (22)$$

334 The abovementioned formula is mainly derived mathematically, often making

335 simplified assumptions about the porous medium model. As a result, there may be

336 some deviation from the actual results.

337 Based on the calculated results of the permeability (Fig. 8), the correlation

338 between the permeability and porosity of the porous media was determined.

339 According to the KC equation (Eq. 19), a linear regression on the relative

340 permeability K and the expression $\varepsilon^3/(1-\varepsilon)^2$ of the porosity was performed. As

341 shown in Fig. 9（a）, R^2 is 0.9876. The largest relative error is 50% when the porosity

342 is 0.35.

To reduce the relative error and obtain a more accurate correlation between permeability and porosity, the logarithms of the relative permeability K and $\varepsilon^3/(1-\varepsilon)^2$ were taken separately, and linear regression was performed to obtain the results shown in Fig. 9(b). The R^2 is 0.9951, which indicates a good degree of fitting. In this study, a new fitting formula is introduced on the basis of the KC formula. The fitting curve is shown in Fig. 10.

$$K = \left(\frac{\varepsilon^3}{(1-\varepsilon)^2}\right)^{0.76} \frac{{d_p}^2}{80} \tag{23}$$

3.2 Effect of particle size distribution on permeability

Soil is composed of particles with different sizes. Smaller particles may have more influence on the permeability due to their greater specific surface area (Liu and Jeng, 2019). Hence, additional investigations have been conducted on correlating the permeability with the particle size distribution. The particle size distribution can be characterized by the gradation parameters. The coefficient of nonuniformity C_u, which reflects the distribution of different particle sizes, can be expressed as

$$C_u = d_{60}/d_{10} \tag{24}$$

To examine the influence of the coefficient of nonuniformity on the permeability, six porous media with different gradation parameters were constructed, and their porosity ε was set to 0.5. The gradation curves for the six porous media are shown in Fig. 11. The relationship between the coefficient of nonuniformity and the relative permeability coefficient is shown in Fig. 12 when the flow is laminar. The results

show that the permeability depends on the coefficient of nonuniformity and increases with an increasing coefficient of nonuniformity, almost with a parabolic trend. Therefore, the effect of the particle size distribution on the permeability is obvious. Equation 25 accounts for the influence of the particle size distribution in the modified KC formula.

$$K = C_1\left(\frac{\varepsilon^3}{(1-\varepsilon)^2}\right)^{0.76} d_p^{\,2} \tag{25}$$

where C_1 is a coefficient related to the coefficient of nonuniformity. It can be expressed separately as

$$C_1 = 0.014C_u^{\,2} - 0.03C_u + 0.022 \tag{26}$$

3.3 Effect of the Reynolds number on permeability

Turbulent flow significantly affects the rate of transport. It comprises a complex flow pattern with various scales of vortices and turbulence structures. This flow state enhances the transport rate within the medium by facilitating mixing and diffusion mechanisms, thereby promoting rapid substance transfer between different regions. Hence, studying turbulent flow helps us better comprehend and control the permeation rate of substances.

The particle Reynolds number (Re) for flow through a porous medium is typically expressed as

$$Re = \frac{VD}{\nu} \tag{27}$$

where D is the medium diameter of the porous medium particles.

385 Flow through soil with a particle Reynolds number less than 1 is classified as
386 laminar, while flow with a particle Reynolds number greater than 100 is considered
387 turbulent. Flow that falls between these two limits is transient. In this study, several
388 simulations were conducted with varying particle Reynolds numbers in the range of
389 0.001 to 3,000 (0.001, 0.01, 001, 0.3, 30, 100, 300, and 3000). Figure 13 demonstrates
390 that the dimensionless permeability remains constant in the laminar regime and does
391 not vary as the particle Reynolds number increases. However, as the particle Reynolds
392 number enters the transient regime, the dimensionless permeability decreases. This
393 finding is consistent with the conclusions drawn in Fattahi's research (Fattahi et al.,
394 2016). Therefore, the empirical formula of permeability needs to consider the effect of
395 the Reynolds number.

396 The Forchheimer term (Eq. 2) is commonly employed to describe the impact of
397 nonlinear drag in turbulent flow. The Forchheimer coefficient β is an empirical
398 coefficient that relies on soil and flow characteristics. The commonly used empirical
399 formula of the Forchheimer coefficient β can be written as

400 $$\beta = \beta_0 \times \frac{1-\varepsilon}{\varepsilon^3} \times \frac{1}{d_{50}} \tag{28}$$

401 where β_0 is an empirical parameter.

402 In previous studies, researchers did not account for the variation in the
403 Forchheimer coefficient with the Reynolds number. Based on Eq. 2, the Forchheimer
404 coefficient β can be calculated. Fig. 14 demonstrates the relationship between the
405 particle Reynolds number and the Forchheimer coefficient. As the velocities increase,

406 the Forchheimer coefficient decreases. The fitting formula of the Forchheimer
407 coefficient is provided below:

408 $$\beta = (-0.006\ln(Re_p) + 0.051) \times \frac{1-\varepsilon}{\varepsilon^3} \times \frac{1}{d_{50}} \quad (29)$$

409 Under turbulent conditions, the fluid demonstrates an irregular velocity
410 distribution and exhibits vortex structures accompanied by highly intricate streamlines.
411 The irregularity of turbulence leads to significant variations in path and velocity as the
412 fluid traverses the pores of the medium, resulting in relatively low permeability.

413 On the other hand, laminar flow describes an ordered and parallel flow state of
414 the fluid within a porous medium. In laminar flow, the fluid displays a layered and
415 parallel velocity distribution with relatively regular streamlines. The ordered nature of
416 laminar flow results in minimal changes in path and velocity as the fluid passes
417 through the medium's pores, leading to relatively high permeability.

418 Based on the above conclusion, a modified Darcy formula considering the size
419 distribution of particles and particle Reynolds number is finally presented. When the
420 particle Reynolds number is less than 1, which indicates that the flow is laminar, Eq.
421 30 is applicable.

422 $$-\frac{dP}{dx} = \frac{1}{K} \cdot (\mu \cdot V) \quad (30)$$

423 $$K = C_1 \left(\frac{\varepsilon^3}{(1-\varepsilon)^2}\right)^{0.76} {d_p}^2 \quad (31)$$

424 where C_1 is a coefficient related to the coefficient of nonuniformity. It can be
425 expressed separately as

426 $$C_1 = 0.014{C_u}^2 - 0.03C_u + 0.022 \quad (32)$$

When the particle Reynolds number is greater than 1, which indicates that the flow gradually becomes turbulent, Eq. 33 is applicable. *K* refers to the same value as Eq. 31.

$$-\frac{dP}{dx}=\frac{1}{K}\cdot(\mu\cdot V)+\beta\cdot(\rho\cdot V^2) \tag{33}$$

$$\beta=(-0.006\ln(Re_p)+0.051)\times\frac{1-\varepsilon}{\varepsilon^3}\times\frac{1}{d_{50}} \tag{34}$$

4. Conclusions

A newly developed 3D multiple relaxation time LBM code has been employed to investigate the effects of several issues, such as effective porosity, particle size, particle size distribution and the particle Reynolds number, on the permeability of porous media. Many numerical simulations were performed under different conditions. From the LBM simulations conducted in this study, the following conclusions can be drawn:

(1) The effects of porosity, particle size, particle size distribution and Reynolds number on the permeability were studied in this paper. It was proven that in addition to the influence of porosity and particle size distribution on the permeability, the influence of the Reynolds number on the permeability is obvious and cannot be ignored.

(2) An analysis of the seepage flow field at the pore scale revealed that certain seepage channels within the network exhibit significantly higher velocities than others, indicating the presence of a dominant seepage main channel phenomenon in the network.

(3) Based on the numerical simulation results, a modified Darcy formula considering all the factors was provided.

The permeability coefficient formula is a valuable tool for future simulations of macroscopic porous seepage models. By integrating this coefficient into numerical models or simulations, we can effectively simulate and analyse the fluid behaviour within porous media under different conditions.

Acknowledgements

The authors gratefully acknowledge the financial support from the National Key Research and Development Project of China (2021YFB2601100), the National Natural Science Foundation of China (51979190), and the Open Funds of State Key Laboratory of Hydraulic Engineering Simulation and Safety of China (Grant No. HESS-2221).

Data Availability Statement

The data for the results presented is available, and the results can be reproduced, using a Docker container available at https://dx.doi.org/10.5281/zenodo.10005571 (Zhang & Li, 2023)

References

Ahmadi, M.M., Mohammadi, S., Hayati, A.N., (2011). Analytical derivation of tortuosity and permeability of monosized spheres: A volume averaging approach.

Physical Review E, 83, 026312. https://doi.org/10.1103/PhysRevE.83.026312

Bogdanov, I.I., Mourzenko, V. V., Thovert, J.F., Adler, P.M., (2003). Effective permeability of fractured porous media in steady state flow. *Water Resources Research*, 39, 1-13. https://doi.org/10.1029/2001WR000756

Carman, P.C., (1939). Permeability of saturated sands, soils and clays. *The Journal of Agricultural Science*, 29(2), 262–273. https://doi.org/10.1017/S0021859600051789

Carman, P. C. (1997). Fluid flow through granular beds. *Chemical Engineering Research and Design*, 75, S32–S48. https://doi.org/10.1016/S0263-8762(97)80003-2

Chen, S., Doolen, G.D.,（1998). Lattice Boltzmann method for fluid flows. *Annual Review of Fluid Mechanics*, 30, 329–364. https://doi.org/10.1146/annurev.fluid.30.1.329

Chukwudozie, C., Tyagi, M., (2013). Pore scale inertial flow simulations in 3-D smooth and rough sphere packs using lattice Boltzmann method. *Transport Phenomena and Fluid Mechanics*, 59, 4858–4870. https://doi.org/10.1002/aic.14232

Despois, J.F., Mortensen, A., (2005). Permeability of open-pore microcellular materials. *Acta Materialia*, 53, 1381–1388. https://doi.org/10.1016/j.actamat.2004.11.031

D'Humières, D., Ginzburg, I., Krafczyk, M., Lallemand, P., Luo, L.S., (2002). Multiple-relaxation-time lattice Boltzmann models in three dimensions. *Mathema*

tical, Physical and Engineering Sciences, 360, 437–451. https://doi.org/10.1098/rsta.2001.0955

Dorai, F., Moura Teixeira, C., Rolland, M., Climent, E., Marcoux, M., Wachs, A., (2015). Fully resolved simulations of the flow through a packed bed of cylinders: Effect of size distribution. *Chemical Engineering Science*, 129, 180–192. https://doi.org/10.1016/j.ces.2015.01.070

Du, R., Shi, B., Chen, X., (2006). Multi-relaxation-time lattice Boltzmann model for incompressible flow. *Physics Letters A*, 359, 564–572. https://doi.org/10.1016/j.physleta.2006.07.074

Fattahi, E., Waluga, C., Wohlmuth, B., Rüde, U., Manhart, M., Helmig, R., (2016). Lattice Boltzmann methods in porous media simulations: From laminar to turbulent flow. *Computers & Fluids*, 140, 247–259. https://doi.org/10.1016/j.compfluid.2016.10.007

Garcia, X., Akanji, L.T., Blunt, M.J., Matthai, S.K., Latham, J.P., (2009). Numerical study of the effects of particle shape and polydispersity on permeability. *Physical Review E*, 80, 021304. https://doi.org/10.1103/PhysRevE.80.021304

Ghassemi, A., Pak, A., (2011). Pore scale study of permeability and tortuosity for flow through particulate media using Lattice Boltzmann method. *International Journal for Numerical and Analytical Methods in Geomechanics*, 35, 886–901. https://doi.org/10.1002/nag.932

Ginzburg, I., d'Humières, D., (2003). Multireflection boundary conditions for lattice Boltzmann models. *Physical Review E*, 68, 066614. https://doi.org/10.1

514 103/PhysRevE.68.066614
515 Ginzburg, I., Verhaeghe, F., dHumières, D., (2008). Two-relaxation-time Lattice
516 Boltzmann scheme: about parametrization, velocity, pressure and mixed bou
517 ndary conditions. *Communications in Computational Physics*, 3, 427-478.
518 Guo, Z., Shi, B., Wang, N., (2000). Lattice BGK Model for Incompressible Na
519 vier-Stokes Equation. *Journal of Computational Physics*, 165, 288–306. htt
520 ps://doi.org/10.1006/jcph.2000.6616
521 Hasanov, A.K., Dugan, B., Batzle, M.L., (2020). Numerical Simulation of Oscil
522 lating Pore Pressure Experiments and Inversion for Permeability. *Water Res*
523 *ources Research*, 56, 1-16. https://doi.org/10.1029/2019WR025681
524 Koponen, A., Kataja, M., Timonen, J., (1996). Tortuous flow in porous media.
525 *Physical Review E*, 54, 406–410. https://doi.org/10.1103/PhysRevE.54.406
526 Koponen, A., Kataja, M., Timonen, J., (1997). Permeability and effective porosi
527 ty of porous media. *Physical Review E*, 56, 3319–3325. https://doi.org/10.1
528 103/PhysRevE.56.3319
529 Krafczyk, M., Tölke, J., Luo, L.S., (2012). Large-eddy simulations with a multi
530 ple-relaxation-time LBE model. *International Journal of Modern Physics B*,
531 17, 33-39. https://doi.org/10.1142/S0217979203017059
532 Lee, S.L., Yang, J.H., (1997). Modeling of Darcy-Forchheimer drag for fluid fl
533 ow across a bank of circular cylinders, *International Journal of Heat and*
534 *Mass Transfer*, 40(13), 3149-3155. https://doi.org/10.1016/S0017-9310(96)00
535 347-X

536 Liu, G., Zhang, J., Zhang, Q., (2021). A high-performance three-dimensional lat
537 tice Boltzmann solver for water waves with free surface capturing. *Coastal*
538 *Engineering*, 165, 1-23. https://doi.org/10.1016/j.coastaleng.2021.103865
539 Li, Y., LeBoeuf, E.J., Basu, P.K., Mahadevan, S., (2005). Stochastic modeling
540 of the permeability of randomly generated porous media. *Advances in Wat*
541 *er Resources*, 28, 835–844. https://doi.org/10.1016/j.advwatres.2005.01.007
542 Liu, Y.F., Jeng, D.S., (2019). Pore scale study of the influence of particle geo
543 metry on soil permeability. *Advances in Water Resources*, 129, 232–249. ht
544 tps://doi.org/10.1016/j.advwatres.2019.05.024
545 Maier, R.S., Kroll, D.M., Kutsovsky, Y.E., Davis, H.T., Bernard, R.S., (1998).
546 Simulation of flow through bead packs using the lattice Boltzmann method.
547 *Physics of Fluids*, 10, 60–74. https://doi.org/10.1063/1.869550
548 Matyka, M., Khalili, A., Koza, Z., (2008). Tortuosity-porosity relation in porous
549 media flow. *Physical Review E*, 78(2), 026306. https://doi.org/10.1103/PhysRe
550 vE.78.026306
551 McNamara, G.R., Zanetti, G., (1988). Use of the Boltzmann equation to simulate
552 Lattice-Gas Automata. *Physical Review Letters*, 61, 2332–2335. https://doi.or
553 g/10.1103/PhysRevLett.61.2332
554 Okabe, H., Blunt, M.J., (2004). Prediction of permeability for porous media rec
555 onstructed using multiple-point statistics. *Physical Review E*, 70(6), 066135.
556 https://doi.org/10.1103/PhysRevE.70.066135
557 Osiptsov, A.A., (2017). Hydraulic fracture conductivity: effects of rod-shaped

proppant from lattice-Boltzmann simulations and lab tests. *Advances in Water Resources*, 104, 293–303. https://doi.org/10.1016/j.advwatres.2017.04.003

Pape, H., Clauser, C., Iffland, J., (2000). Variation of Permeability with Porosity in Sandstone Diagenesis Interpreted with a Fractal Pore Space Model. *Pure and Applied Geophysics*, 157, 603-619. https://doi.org/10.1007/PL00001110

Rodríguez, E., Giacomelli, F., Vazquez, A., (2004). Permeability-porosity relationship in RTM for different fiberglass and natural reinforcements. *Journal of Composite Materials*, 38, 259–268. https://doi.org/10.1177/0021998304039269

Saomoto, H., Katagiri, J., (2015). Particle Shape Effects on Hydraulic and Electric Tortuosities: A Novel Empirical Tortuosity Model Based on van Genuchten-Type Function. *Transport in Porous Media*, 107, 781–798. https://doi.org/10.1007/s11242-015-0467-z

Scholes, O.N., Clayton, S.A., Hoadley, A.F.A., Tiu, C., (2007). Permeability anisotropy due to consolidation of compressible porous media. *Transport in Porous Media*, 68, 365-387. https://doi.org/10.1007/s11242-006-9048-5

Sheikh, B., Pak, A., (2015). Numerical investigation of the effects of porosity and tortuosity on soil permeability using coupled three-dimensional discrete-element method and lattice Boltzmann method. *Physical Review E*, 91(5), 053301. https://doi.org/10.1103/PhysRevE.91.053301

Sobieski, W., Trykozko, A., (2014). Darcy's and Forchheimer's laws in practice. Part 1. The experiment, Technical Sciences, 17(4), 321-335.

Stefansson, I., Keilegavlen, E., (2023). Numerical Treatment of State-Dependent P

ermeability in Multiphysics Problems. *Water Resources Research*, 59, 1-14. https://doi.org/10.1029/2023WR034686

Stewart, M.L., Ward, A.L., Rector, D.R., (2006). A study of pore geometry effects on anisotropy in hydraulic permeability using the lattice-Boltzmann method. *Advances in Water Resources*, 29, 1328–1340. https://doi.org/10.1016/j.advwatres.2005.10.012

Torskaya, T., Shabro, V., Torres-Verdín, C., Salazar-Tio, R., Revil, A., (2014). Grain shape effects on permeability, formation factor, and capillary pressure from pore-scale modeling. *Transport in Porous Media*, 102, 71–90. https://doi.org/10.1007/s11242-013-0262-7

Williams, S.R., Philipse, A.P., (2003). Random packings of spheres and spherocylinders simulated by mechanical contraction. *Physical Review E*, 67, 051301. https://doi.org/10.1103/PhysRevE.67.051301

Wilson, A.M., Huettel, M., Klein, S., (2008). Grain size and depositional environment as predictors of permeability in coastal marine sands. *Estuarine, Coastal and Shelf Science*, 80, 193–199. https://doi.org/10.1016/j.ecss.2008.06.011

602

603

604 Table 1 Simulation Parameters Used in Section 2.3

Parameter	Value
Fluid density	994.49 kg/m^3
Dynamic viscosity coefficient	0.000743 kg/m·s
Kinematic viscosity coefficient	0.000000747m^2/s
Porosity of porous media	0.37
Medium particle size of porous media	1.95 mm
Nonuniformity coefficient	1.1
Water velocity range	0.00002-0.01 m/s

605

606

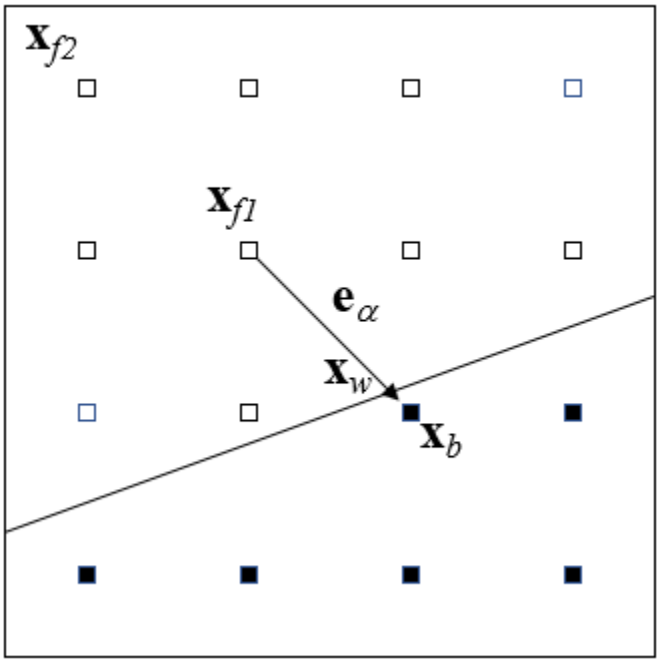

607 Fig. 1. A two-dimensional example of the boundary node, where $\mathbf{X}_f$ represents fluid

608 node and $\mathbf{X}_b$ represents solid node.

609

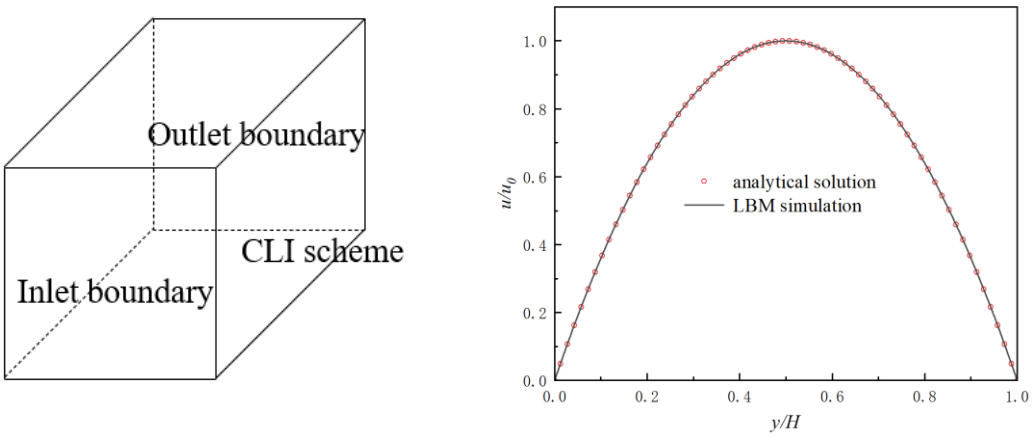

610

611 Fig. 2. (a) The simulation domain of the numerical model, where the inlet boundary

612 and outlet boundary using the pressure boundary condition. And the CLI boundary

613 condition is used for the other four boundaries. (b) Comparison between LBM

614 simulation and analytical solution of Poiseuille flow (Eq.13).

615

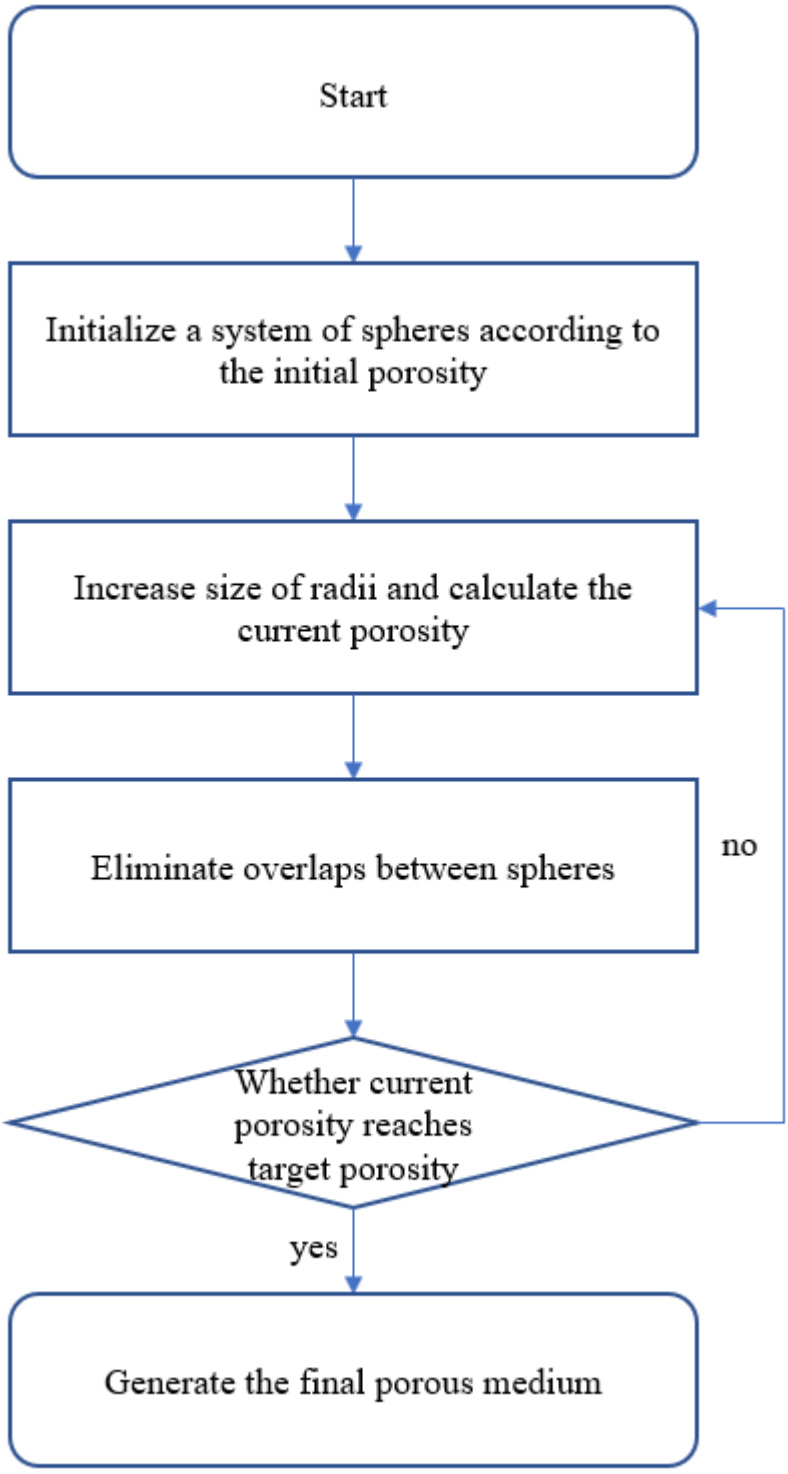

Fig. 3. Flowchart of the generation of porous medium

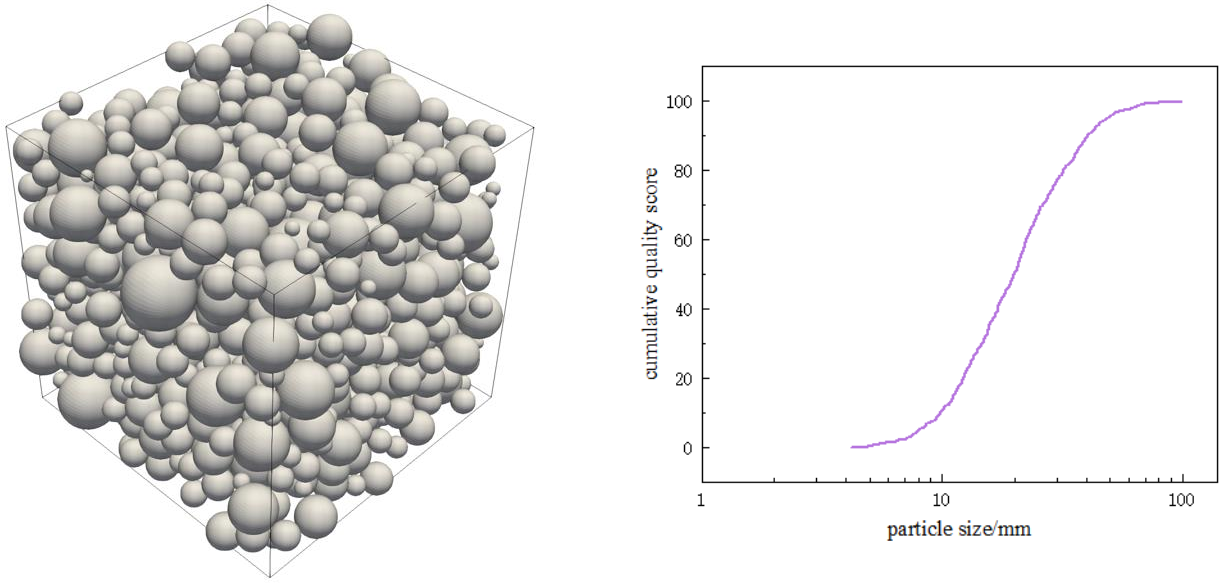

619

620 Fig. 4. (a) Porous medium is constructed using the code, where the porosity of porous

621 medium is 0.5 and the particle number is 1000. (b) Particle size distribution of the

622 generated porous medium.

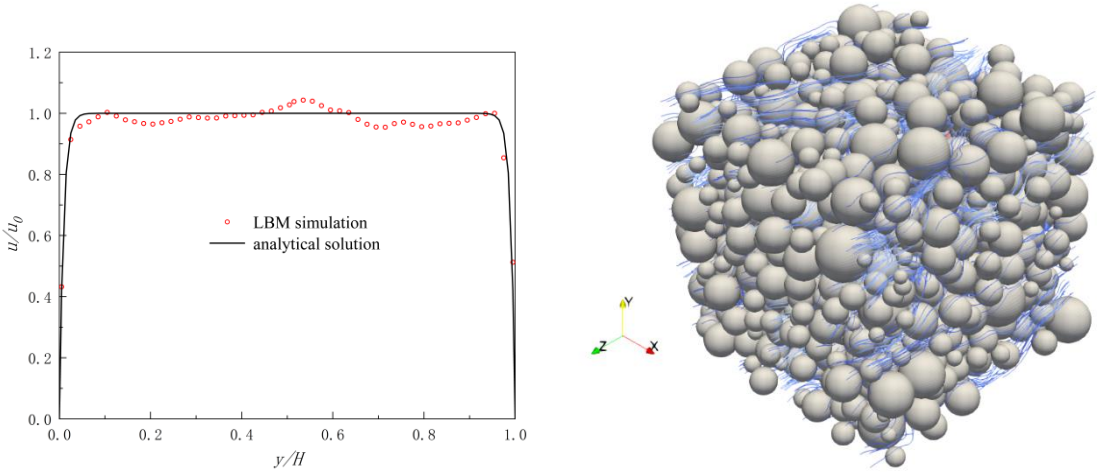

623

624 Fig. 5. (a) Comparison between LBM simulation and analytical solution of porous

625 Poiseuille flow (Eq.18) with porosity of 0.5.(b) Streamlines of flow through spherical

particles in porous Poiseuille flow

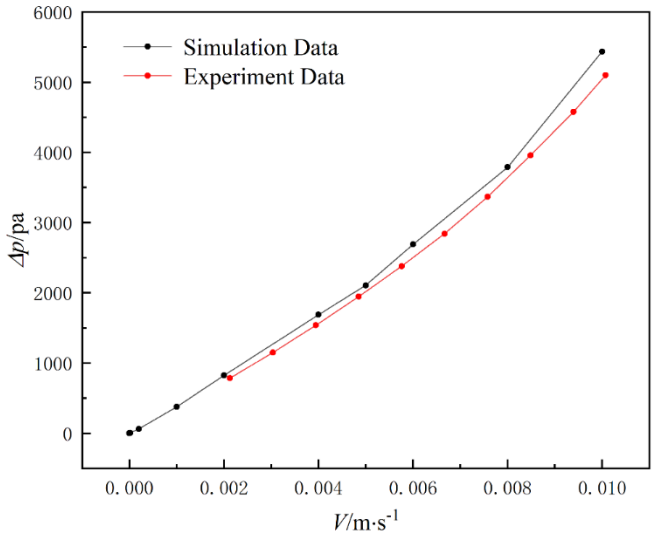

Fig. 6. Comparison between experimental data by Sobieski and Trykozko (2014) and simulation data

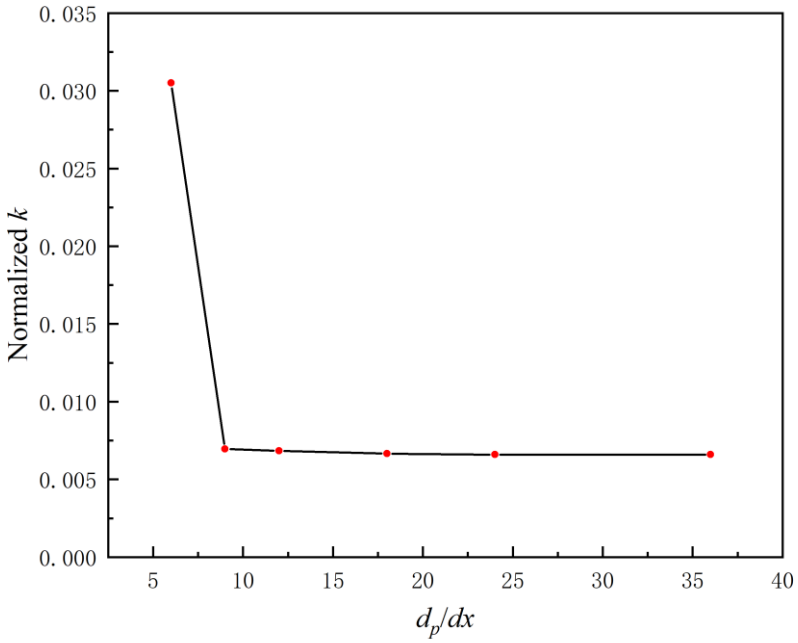

Fig. 7. Permeability of spherical particles with different resolutions with porosity of

632 0.5.

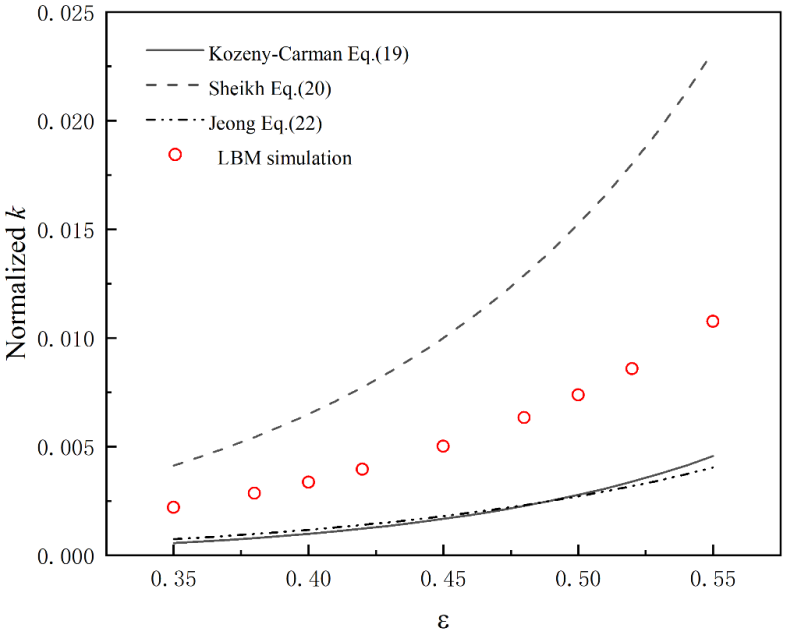

633

634 Fig. 8. Comparison between simulation results and other empirical formulas

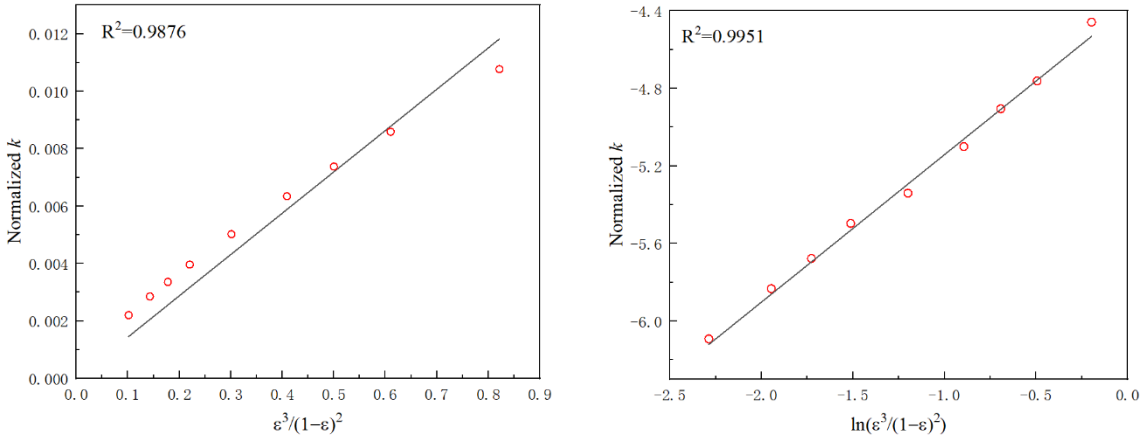

635

636 Fig. 9. (a) Linear regression on the relative permeability K and the expression

637 $\varepsilon^3/(1-\varepsilon)^2$ of the porosity. (b) Linear regression on the relative permeability K and

638 the expression $\ln(\varepsilon^3/(1-\varepsilon)^2)$ of the porosity.

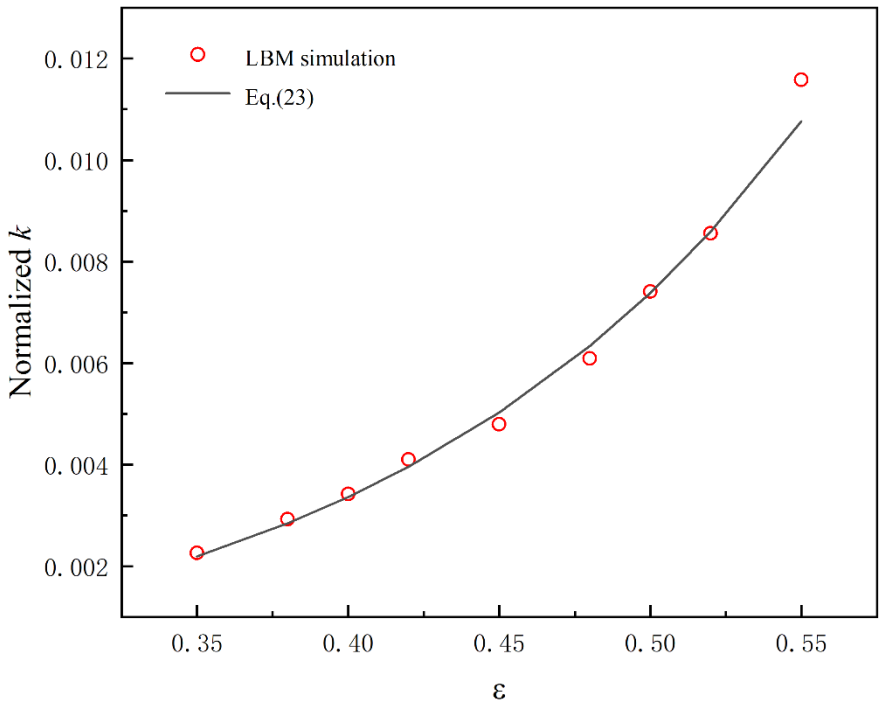

Fig. 10. Simulation results and the empirical formula

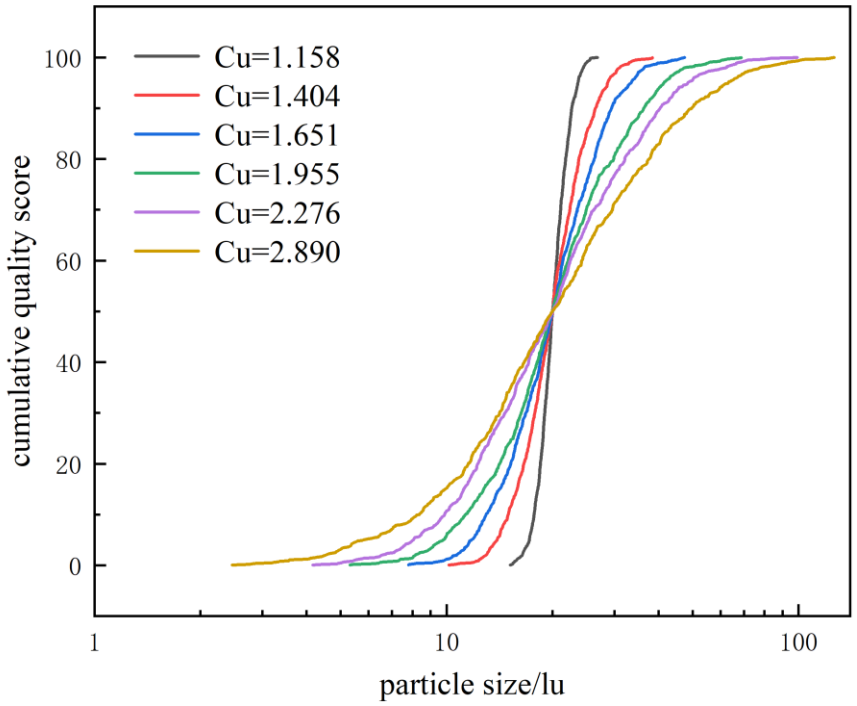

645

646 Fig. 11. Gradation curves for different calculation cases

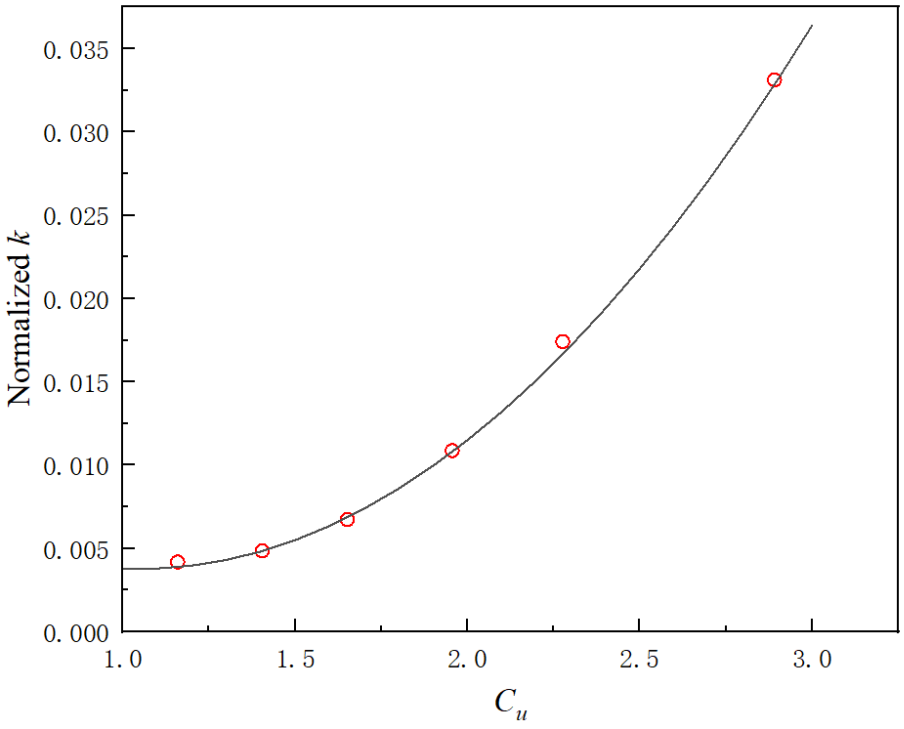

647

648 Fig. 12. Relation between the relative permeability coefficient and coefficient of

649 nonuniformity with porosity of 0.5.

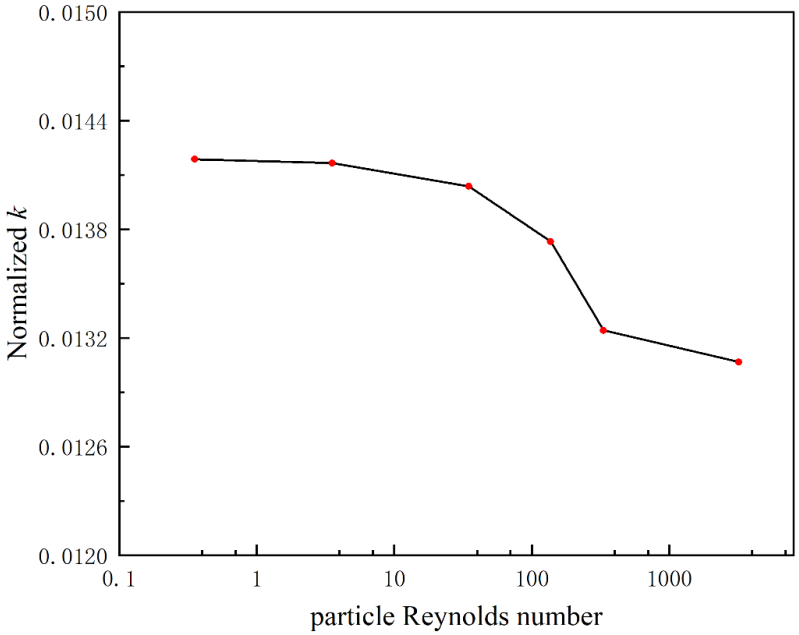

650

651 Fig. 13. Permeability with different particle Reynolds numbers with porosity of 0.4.

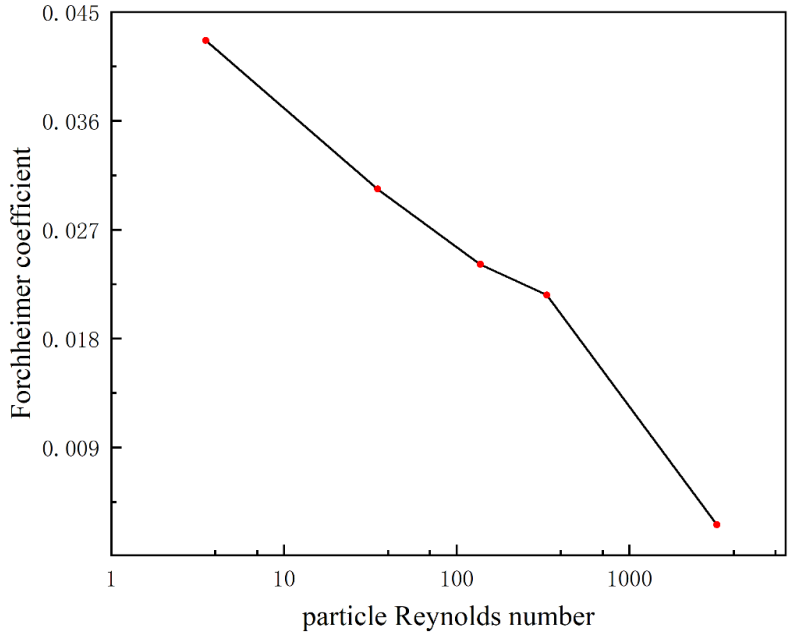

652

653 Fig. 14 Permeability with different particle Reynolds numbers with porosity of 0.4.